Journal of Thermal Analysis and Calorimetry (2020) 139:1717–1729
https://doi.org/10.1007/s10973-019-08563-4

Boric acid (H_3BO_3) as flux agent of clay-based ceramics, B_2O_3 effect in clay thermal behavior and resultant ceramics properties

M. F. Hernández[1,2] · M. A. Violini[1,2] · M. F. Serra[1] · M. S. Conconi[1,2] · G. Suarez[1,2] · N. M. Rendtorff[1,2]

Received: 13 December 2018 / Accepted: 4 July 2019 / Published online: 29 July 2019

Abstract
Ceramic materials were satisfactorily processed through a dry scalable process from binary clay–boric acid (H_3BO_3) mixtures. Relevant thermal parameters were established by a multitechnique approach that included thermogravimetric, differential thermal analysis, dilatometric analysis and structural and microstructural characterization of fired samples. Both clay and boric acid thermal processes were described and correlated. The experimental textural properties evidenced a porosity decrease with sintering temperature and acid addition in the 1100–1300 °C range. The amount of glass was strongly increased by the boron oxide incorporation, confirming its fluxing capacity. X-ray diffraction, supplemented by Rietveld–Le Bail refinement, verified the presence and thermal evolution of crystalline and glassy phases. The observed microstructure was similar to other clay-based ceramics, with quartz, cristobalite and mullite grains imbibed in the silica-based glassy phase. The observed mullite phase was actually a boron mullite solid solution. Boric acid was confirmed as an adequate boron oxide source. The present study gives information for further clay-based materials design with boron oxide as fluxing agent. The dry route hypothesis was confirmed. Both formulation and firing programs can be optimized. High boron addition (5 mass%) is not recommended due to the observed partial rehydration.

Keywords Clay-based material · Boric acid · Dry route · Thermal behavior

Introduction

In kaolinitic clays, the principal crystalline phase is kaolinite (K: $Al_2O_3{\cdot}2SiO_2{\cdot}2H_2O$), and it is usually present with other phases like quartz, feldspars and titania [1–3]. The kaolinite thermal transformations are affected by heating treatments (rate, dwell and atmosphere) and presence of impurities as well as additives and particle size [4].

Kaolinitic clays are utilized in a large variety of industrial applications such as ceramics, refractories, cement, filling agent in paper, plastics, rubber and cosmetics in order to reach the desired properties. Thermal treatments are involved in the majority of these applications [5–10]. Ceramic industry might be one of the most important in terms of volume.

Energy consumption is one of the most important factors in ceramic production as far as cost is concerned. This fact becomes critical when the material needs to be sintered at high temperatures (higher than 1200 °C). Any contribution in the way of reducing energy requirement is of importance [11, 12].

At present, the existing environmental and economic conditioning factors, the need for better use of natural resources and to reuse the wastes generated in the own manufacturing processes, among other factors, are driving the search for alternative products and processes that allow both efficiency and sustainability criteria nowadays demanded by society. This search implies the reformulation of current compositions by the incorporation of new raw materials or additives. Similarly, rising deflocculant costs may be offset by the design of compositions with lower clay material contents and small quantities of binder [13].

✉ M. F. Hernández
florenciahernandez@cetmic.unlp.edu.ar

[1] CETMIC Centro de Tecnología de Recursos Minerales y Cerámica (CIC-CONICET La Plata), Cno. Centenario y 506 s/n, M.B. Gonnet (1897), Buenos Aires, Argentina

[2] Departamento de Química, Facultad de Ciencias Exactas, Universidad Nacional de La Plata, 47 y 115 s/n, La Plata (1900), Buenos Aires, Argentina

Boron compounds have been proposed as complementary raw materials in several ceramic manufactures [14–16], with a high fluxing behavior, which might low the firing programs in ceramics manufacture, with consequent energy savings [17–19]. Boron minerals like borax ($Na_2[B_4O_5(OH)_4].8H_2O$), colemanite ($Ca_2B_6O_{11}.5H_2O$), ulexite ($NaCaB_5O_9{\cdot}8H_2O$), hidroboracite ($CaMg[B_3O_4(OH)_3]_2.3H2O$) and boric acid ($H_3BO_3$) are usually employed as raw materials for frits glaze manufacturing [20]. During frit processing, no solubility problem arises. On the other side, during wet milling (and mixing) the solubility is indeed a problem. Remarkably, one of the mentioned energy consumption optimization strategies is dry grinding and granulation [11]. In this, the powders used for the manufacture of tiles by dry pressing need to have good flow properties and a well-mixed, uniform composition which is usually achieved by spray drying of the ceramic slip, where the powders form large spherical agglomerates. Instead of spray drying, agglomerates can be formed by dry grinding and granulation. First the raw materials are almost completely dried by a hot air stream and then are dry ground. In order to achieve granulation, the dry ground powder is mixed with a very fine spray of water to provide moisture content of up to roughly 10%. Then, the material is agglomerated with the aid of the rotational movement of the granulator. In this way, energy savings result from the reduction in the amount of water to be evaporated in the subsequent drying process. Assuming that the raw material has a 6% moisture content, dry grinding and granulation result in a specific energy consumption roughly 2.5 times less than that for wet grinding and spray drying (0.7 vs. 1.8 GJ t^{-1}) [11, 21, 22].

Recent studies, which have also sought to reduce manufacturing costs, have attempted to shorten the porcelain tile firing cycle by introducing highly fluxing additives [23] or wastes [19, 24, 25]. Boric acid falls within this strategy as well. No systematic boron oxide-clay thermal studies have been reported, and in this article, we fulfill this gap.

The objective of the present article is to study the effect of the boron oxide in the thermochemical processes and ceramic behavior of one industrial kaolinitic clay.

In this work, we describe the effect of boric acid addition to the thermal behavior of an industrial kaolinitic clay and evaluate the changes in the technological properties of the resulting ceramics, using differential thermal analysis (DTA), thermogravimetric analysis (TG), dilatometric analysis (TMA) and conventional X-ray powder diffraction (XRD) with Rietveld refinement.

This will enlighten the processing strategy of boric acid-based ceramic applicable in a dry processing route.

Experimental

Raw materials

An industrial kaolinitic ball clay from Santa Cruz (Tincar S, PG La Toma Argentina) [26], Argentina, and commercial boric acid (Borax Argentina SA, Argentina) with 99.8% of H_3BO_3 (56.2% B_2O_3), CAS No.: 10043-35-3, were used as raw materials. Boric acid was dry-milled in a disk and ring mill (Herzog HS-100). The chemical and mineralogical composition is shown in Table 1.

The alumina content and the low alkali content (below 2.5%) confirm the refractoriness of the clay. The mineralogical composition (XRD-Rietveld) confirms the kaolinitic denomination of the studied clay [2]. This phase is accompanied principally by quartz.

Preparation of starting mixtures

Three compositions with 1, 3 and 5 mass% of elemental boron (B) were studied starting from boric acid. They were labeled T-Ac1, T-Ac3 and T-Ac5, respectively; samples without acid addition were labeled T. Dry milling was employed for avoiding solubility problems of the boric acid. A planetary ball mill was employed (Fritsch Pulverisette premium line 7). Zirconia jars (85 mL) and milling elements (10 mm diameter) were employed. Both the pure industrial clay and the mixtures were subjected to equivalent mixing-milling pretreatments. Afterward, disk shape samples were uniaxially pressed (15 mm diameter and $\approx$ 3 mm height) up to 100 MPa. These were sintered in electric furnace, with air atmosphere, with 5 °C min^{-1}

Table 1 Chemical and mineralogical composition in mass basis of the Tincar clay (XRF)

Tincar	Kaolinitic clay/mass%
Chemical composition	
LOI	7.63
SiO_2	61.82
Al_2O_3	27.55
Fe_2O_3	0.79
MgO	0.66
K_2O	0.76
Na_2O	–
TiO_2	0.39
CaO	0.28
Mineralogical composition	
Kaolinite	59.0
Quartz	41.0

heating rate and 60 min soaking, with maximum temperatures between 1100 and 1400 °C.

Sample characterizations

The thermal behavior of the mixtures was studied applying thermogravimetric (TG) and differential thermal analyses (DTA) and dilatometry (TMA) which were performed up to 1400 °C. Both thermal analyses were carried out simultaneously at a 5 °C min^{-1} heating rate in air atmosphere (TG–DTA and TMA Rigaku Evo plus II, Japan). The TG–DTA analysis of the boric acid and the clay was also performed to understand the chemical behavior of this starting powder.

After this analysis, samples were fired at the same heating rate (5 °C min^{-1}) with different maximum temperatures in the range of 1100–1400 °C and 30 min soaking in air atmosphere.

The crystalline phases of sintered samples were determined by X-ray diffraction (XRD) using CuKα radiation operating at 40 kV and 30 mA (Philips PW1710). The XRD patterns were analyzed with the program FullProf (version 4.90, July 2010), which is a multipurpose profile-fitting program [27, 28], including Rietveld–Le Bail refinement to perform phase quantification [29, 30].

Once the sintering program was optimized, the linear shrinkage was measured; the green and sintered volumetric density was calculated from the volume: mass ratio. Archimedes immersion method was also carried out in the range 1100–1400 °C.

Finally in order to describe the developed microstructures, a microstructural analysis was performed by a scanning electron microscope (SEM) (JEOL, JCM-6000).

Results and discussion

Thermal behavior of the raw materials: clay and boric acid

Figure 1 shows TG and DTG, DTA and the TMA. Generally, these present an expected typical behavior of kaolinitic clay. In the TG-DTG analysis of the clay, the typical two mass losses can be observed in the 0–1400 °C range: The first one (≈ 1%), below 150 °C, corresponds to the surface water loss. The second one (≈ 7%) mass loss corresponds to the kaolinite decomposition (dehydroxylation) into metakaolinite (MK: $Al_2Si_2O_5$) (also *a* water loss) [31]. This analysis permits to identify the transformation temperature. No other mass loss (or gain) process occurs in this temperature range. In the DTA curve, both endothermic and exothermic processes can be detected. The mass loss is in accordance with the mineralogical

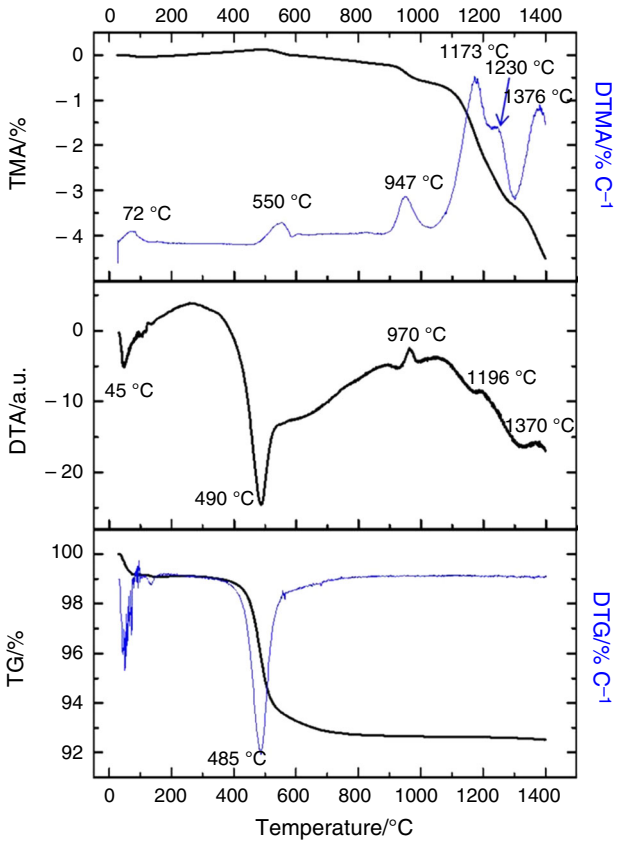

Fig. 1 Thermal behavior of the Tincar clay (TG, DTG, DTA, TMA and DTMA)

composition evaluated by XRD-Rietveld. Besides the named processes, the kaolinite–quartz system presents the allotropic quartz transformation ($\alpha \rightarrow \beta$) that occurs at 573 °C [2].

The surface water loss presents an endothermic process, centered at 150 °C. A broad endothermic band centered at 538 °C, due to clay dehydroxylation reaction that is overlapped with $\alpha \rightarrow \beta$ quartz transformation with less energy involved, is the most important peak of the DTA analysis. The observed temperatures correspond to the TG ones and the previously reported ones [3, 4]. An exothermic peak is observed centered at 986 °C; this corresponds to the metakaolinite transformation into a spinel-type aluminosilicate (SAS) [32] (Table 2). At higher temperatures, a small and wide exothermic peak was measured in the 1200–1300 °C range, and this corresponds to the mullite formation [33]. Again, the detected temperatures correspond to the ones observed for similar materials [27–29]. In fact, this wide peak consists in a couple of overlapped peaks centered at 1230 °C and 1250 °C that may correspond to both mullitization pathways (solid-state transformations and crystallization) [34, 35].

The thermal behavior of the boric acid presents a set of consecutive reactions that involve mass (water) losses.

Table 2 Thermal parameters of the Tincar clay (T) and clay–boric acid mixtures

Process	Temperature/°C	Mass loss/%			
		T	T-Ac1	T-Ac3	T-Ac5
(a) Surface water loss	40–100	0.9	1.07	1.81	1.74
(b) Boric acid decompostion		–			
(i) $H_3BO_3 \rightarrow HBO_2 + H_2O$	90–170		1.77	2.77	3.37
(ii) $4HBO_2 \rightarrow H_2B_4O_7 + H_2O$			1.18	1.98	5.54
(iii) $H_2B_4O_7 \rightarrow 2B_2O_3 + H_2O$			0.35	3.17	3.95
(c) Quartz allotropic transformation ($\alpha \rightarrow \beta$)	573	–	–	–	–
(d) Kaolinite dehydroxylation					
$Al_2O_3 \cdot 2SiO_2 \cdot 2H_2O\,(K) \rightarrow Al_2O_3 \cdot 2SiO_2(MK) + 2H_2O$	450–570	6.46	6.00	5.63	4.75
(e) Spinel and premullite formation		–	–	–	–
$Al_2O_3 \cdot 2SiO_2(MK) \rightarrow \text{espinel Al} - \text{Si(SAS)}$	980				
$Al_2O_3 \cdot 2SiO_2(MK) \rightarrow 3Al_2O_3 \cdot 2SiO_2(Mi)$					
(f) Secondary mullite formation (Mii)					
$\text{spinel Al} - \text{Si(SAS)} + SiO_2(V) \rightarrow 3Al_2O_3 \cdot 2SiO_2(Mii) + SiO_2(V)$	1200	–	–	–	–
(g) Boron evaporation					
$B_2O_{3(l)} \rightarrow B_2O_{3(g)}$	1250–1400	–	1.66	2.54	3.55

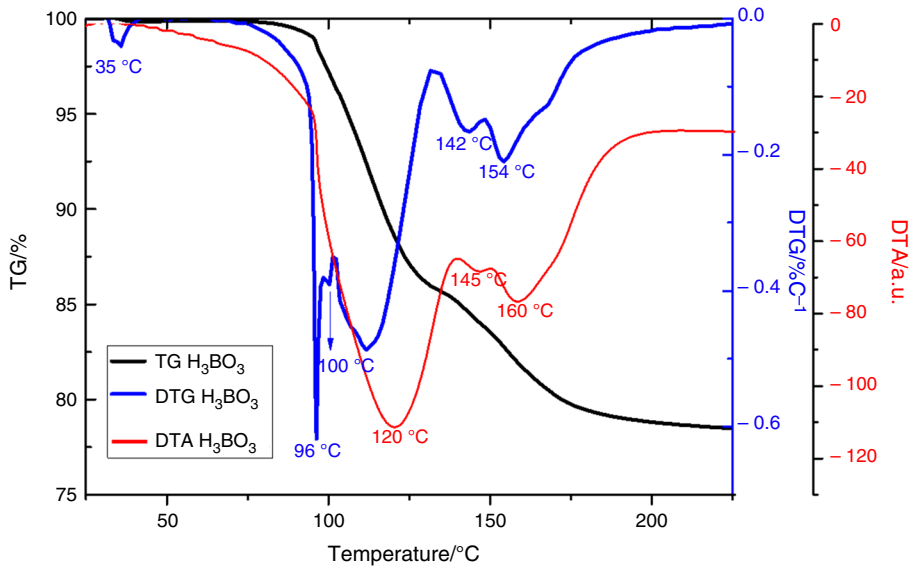

Fig. 2 Thermal behavior of the boric acid (TG, DTG and DTA)

These were correctly evaluated by the combination of the thermogravimetric analysis and the differential thermal analysis (Fig. 2). Values are similar to the ones observed previously [36]. Different metaborates have been proposed as intermediates. Above 200 °C, only boron oxide results from the thermal decomposition. This fact confirms that the acid is an adequate oxide source. Below 200 °C, the clay minerals do not present important thermochemical changes other than surface water loss [1].

Thermal behavior of the clay acid mixtures

A multitechnique approach was carried out for understanding the effect of the boron oxide in the thermochemical processes of the kaolinitic clay, with an employed heating rate of 5 °C min^{-1} for every case. From each analysis, several thermal parameters were defined and associated with the corresponding thermochemical processes: mass losses associated with water or hydroxyl formations, allotropic transformation, crystallizations, etc. Both intensity and temperature were systematically

compared; table forms were also included for better visualization (Table 2). The local maximum or minimum was employed for temperature assignation.

Thermogravimetric and differential thermal analysis (TG–DTA) of the Tincar clay and clay–boric acid mixtures

Figure 3 shows the thermogravimetric curves of the studied mixtures (TG and DTG), Fig. 4 shows the differential thermal analysis curves (DTA), and the pure clay is shown as well.

The thermal parameters are presented in Table 2. The surface water loss (*a*) is observed in all the mixtures, as well as in the non-added sample (endothermic peak), values are similar, and the slight difference might be explained by differences in the drying process.

The multistep boric acid decomposition into boron oxide was observed in the mixtures (processes *b*), in the 90–170 °C range as seen before by other authors [36].

The mass loss is proportional to the added acid, the DTA peaks intensity as well. It could be concluded that the decomposition was not influenced by the clay. This shows that the acid is a proper boron oxide source.

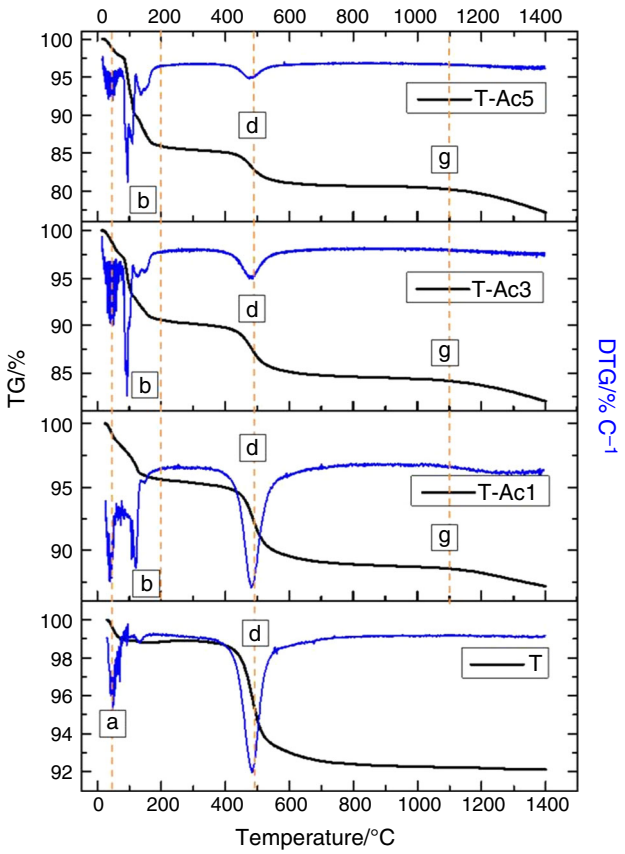

Fig. 3 Thermogravimetric curves of the Tincar clay (T) and clay–boric acid mixtures (T-Ac1; T-Ac3; T-Ac5)

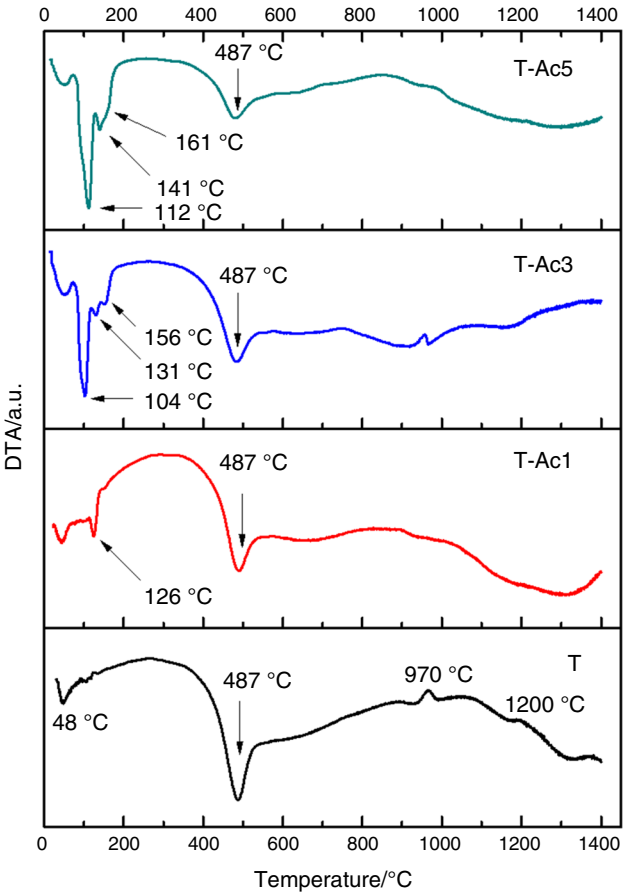

Fig. 4 Differential thermal analysis of the Tincar clay (T) and clay–boric acid mixtures (T-Ac1; T-Ac3; T-Ac5)

The kaolinite (K) dehydroxylation into metakaolinite (MK) can be observed in both TG and DTA [3]. This process (*d*) occurred in the 450–570 °C range for the pure clay and the mixtures. The mass loss change observed is due to the lower clay proportion in the mixtures. From this, it could be inferred that the boron oxides do not affect the kaolinite dehydroxylation.

The quartz transformation (process c) was not observed in the DTA curves, even though the high quartz content ($\approx$ 40%). The associated heat is lower than the heats involved in the other processes.

An exothermic peak is observed centered at 970 °C in the pure clay; this corresponds to the metakaolinite transformation into a spinel type (processes *e*). This is difficult to observe in the clay acid mixtures, as the DTA signal apparently flattens. Evidently, the presence of the boron oxide, melted at this temperature [14, 36], affects the premullite and/or spinel formation [3].

The mullite formation (process *f*) can be observed as a small shoulder in the pure clay (labeled at 1200 °C).

Finally, slight progressive mass loss is observed only in the mixtures above 1200 °C; this can be explained as a

partial evaporation of boron oxides, which was previously observed in alumina boron system [37–39].

Dilatometric analysis (TMA)

The macroscopic thermal behavior of the clay and clay mixtures was recently fully described by Zanelli [40, 41]. The present studied materials revealed a similar behavior (Fig. 5). In this, the first thermal expansion (positive slope in the TMA) range can be observed, from room temperature to 500 °C; this corresponds to the thermal expansion of the clay mineral. At 573 °C, the quartz transformation can be observed (a clear peak in the DTMA curves). This is not affected by the boron oxide incorporation.

After this temperature, a flat zone is observable which finishes with a minor inflection stage at ≈ 980 °C, where an abrupt 1% sigmoidal shrinkage can be observed in the TMA curve and a clear peak in the DTMA curve. These processes can be associated with the DTA spinel formation peak (Fig. 4). After the spinel formation, a slight shrinkage stage can be observed that finishes at 1080 °C; the 980° shrinkage, clearly observed in the pure clay, is slightly observed in the Ac-1 and not observed in the Ac-3 and Ac-5 samples. This peak (DTMA) corresponds to the SAS

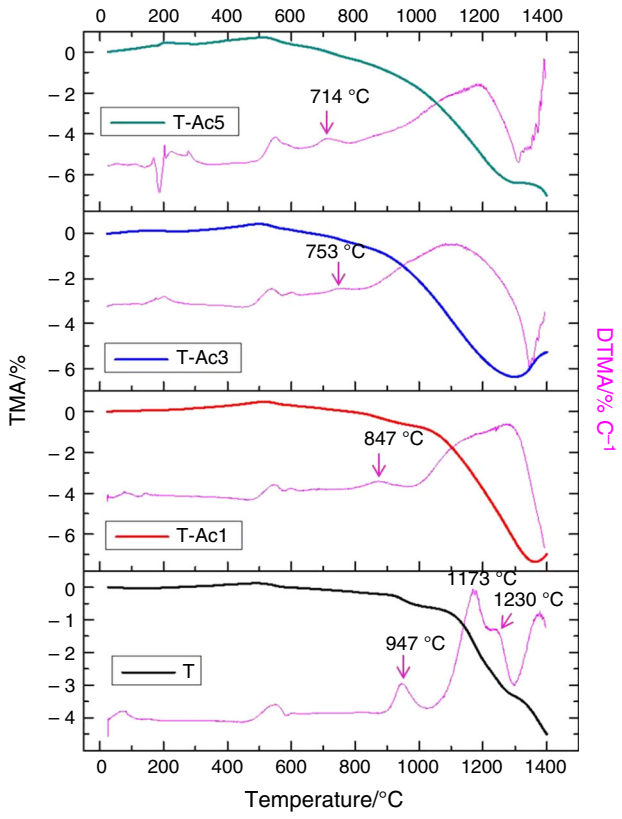

Fig. 5 TMA curves (dilatometry) of the Tincar clay (T) and clay–boric acid mixtures (T-Ac1; T-Ac3; T-Ac5). In all cases, the pink curve represents the derivative of the TMA (DTMA)

formation [32]; this flattens and moves into lower temperatures (down to 714 °C). The liquid boron oxide formed at lower temperatures (Fig. 5) strongly affects the transformation from metakaolinite to SAS. This thermal process consists in the formation of amorphous silica phase and the nanocrystalline spinel phase. The SiO_2–B_2O_3 binary system presents low eutectic point slightly above 500 °C [42]. Hence, the eutectic formation enhances the MK into SAS transformation. This is verified by the temperature decrease in the corresponding DTMA peak, as shown in Fig. 5.

After this processes, the viscous sintering process occurs. This shrinkage consists in a three-step process for the pure clay (T). Three peaks can be devised in the DTMA curve, with easily definable peaks at 947 and 1173 °C and as a shoulder at 1230 °C. This corresponds to the glassy viscous silica-based phase formed by the produced silica originated in the clay decomposition, the SAS formation and the feldspar decomposition accompanied the sintering processes. The mullite formation is observed at higher temperatures (above 1200 °C). The incorporation of boron oxide evidently affects these processes; in fact, the previously formed SiO_2–B_2O_3 glassy phase affects these processes. This low-viscosity phase enhances the sintering processes, and the alkali and earth alkali oxides dissolve into ternary and quaternary glass, which is responsible of the sintering. In this case, the amount of alkali is only provided by the studied industrial clay. This phenomenon would also occur if feldspars or other alkali source are added to the material formulation. During sintering, pores are collapsed, mullite phase is formed, and quartz is partially dissolved by the active multiphase silica-based glass [40] or irreversibly transformed into cristobalite [9]; the XRD analysis is shown below.

The final sinterization temperature, assumed as the local minimum in the TMA curve, follows the T-Ac5 < T-Ac3 < T-Ac1 sequence. The pure fire clay sample does not reach the local minimum in the studied temperature range; the optimum (or maximum) sinterization would only be achieved at higher temperatures. This fact also suggests the fluxing role of the studied additive (boric acid). The completed shrinkage is almost constant for the three samples (≈ 6%). Above this temperature, an over-firing is observed for the three samples. This macroscopic enlargement is accompanied by the formation of gas bubbles, insoluble at this temperature [2, 40].

Sintering parameters: open porosity (P) and apparent density (D)

Sintering advance is usually followed by Archimedes immersion test. Both open porosity (P) and apparent density (D) are determined from these tests. Porosity is strongly related to the mechanical behavior and thermal

insulating properties of ceramics [43–46], which are related to the actual technological applications.

The solely clay-based material porosity decreased from 24 to 14% between 1100 and 1300 °C sintering programs, and a fully densification of these fire clays is only achieved at higher temperatures, but falls out of the present study. This could be achieved by the incorporation of other secondary raw materials, like feldspars or other fluxing agents with the obvious consequence in the complexity of the chemical and thermochemical processes. In order to describe these processes, a binary mixture was chosen.

The obtained ceramics from binary mixtures present a clear tendency. In every case, the boric acid addition resulted in lower porosities, in the 1100–1300 °C range with additions up to 3 mass% This can be clearly observed in Fig. 6, where the open porosity (P) is plotted as a function of the boric acid proportion for the three temperatures studied. Boric acid can be understood as a fluxing agent. Higher additions did not lead to lower porosities. In fact, Ac-5 presented higher porosities compared to samples with a lower addition of boric acid, when fired at 1300 °C. This is an evidence of de-sinterization and a partial boron oxide volatilization (gas bubbles formation), expected at these temperatures. This was also observed in lower proportion at 1200 °C.

The achieved apparent density is within the expected values (Fig. 7) [2]. The pure mineral-based materials (T) fall between 1.95 and 2.08 g cm^{-3}. As expected, higher densities are obtained after higher-temperature programs. A slight increase in the density is observed with 1% additions in the three studied programs. On the other side, higher additions resulted in an important decrease in the density ($\approx$ 1.8 and $\approx$ 1.6 g cm^{-3} for t-Ac3 and T-Ac5 materials), and no important effect of the final temperature was observed, showing that the porosity effects observed in Fig. 6 are only textural changes and not mineralogical changes. The actual crystalline and glassy phase identification and quantification are shown in the following section (Fig. 8).

Crystalline and non-crystalline phase proportions of the developed ceramics fired at 1200 and 1300 °C by the Rietveld method and the Le Bail method

The diffraction patterns show the presence of both crystalline and non-crystalline glassy phases (Fig. 8) [40]. The identified crystalline phases and employed crystallographic cards are shown in Table 3.

The typical silica-based amorphous band can be easily observed in the boron-containing samples. The crystalline phases identified and quantified for the six samples were mullite ($3Al_2O_3{\cdot}2SiO_2$), cristobalite (SiO_2) and quartz (SiO_2).

The shape of the cristobalite peaks could not be satisfactorily fitted by a single contribution. Two different cristobalite structures were proposed for the Rietveld refinement. This was previously proposed for similar materials [47–49]. Refined cell parameters for both cristobalites are shown in Table 4. This might be explained by the coexistence of two dissimilar phases, with different presence of impurities: one produced from the kaolinite thermal decomposition and the other from the thermal transformation of the initial quartz present in the clay mineral, the second one presenting lower impurities content.

It is well known that the vast majority of the AI_2O_3–SiO_2–Re_2O_3 systems (Re: metal) are characterized by their glass-forming abilities [1, 50–52], and the boron element is

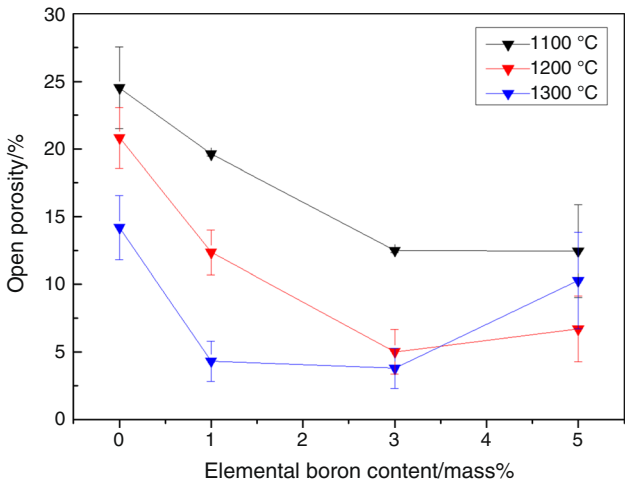

Fig. 6 Open porosity (P) as a function of the boric acid proportion for the different firing programs (1100, 1200, 1300 °C)

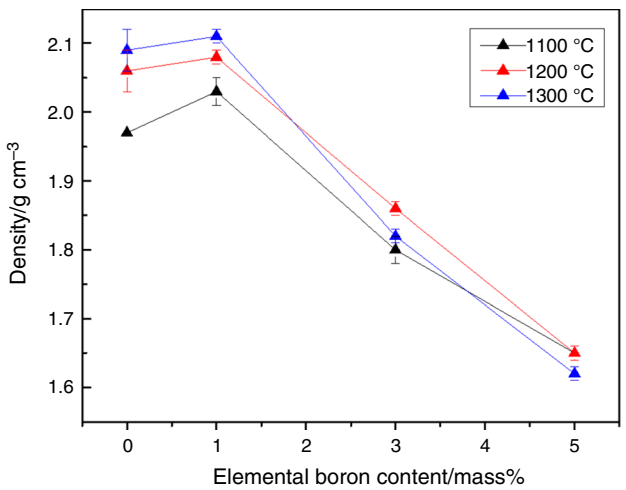

Fig. 7 Apparent density as a function of boric acid proportion for the different firing programs (1100, 1200, 1300 °C)

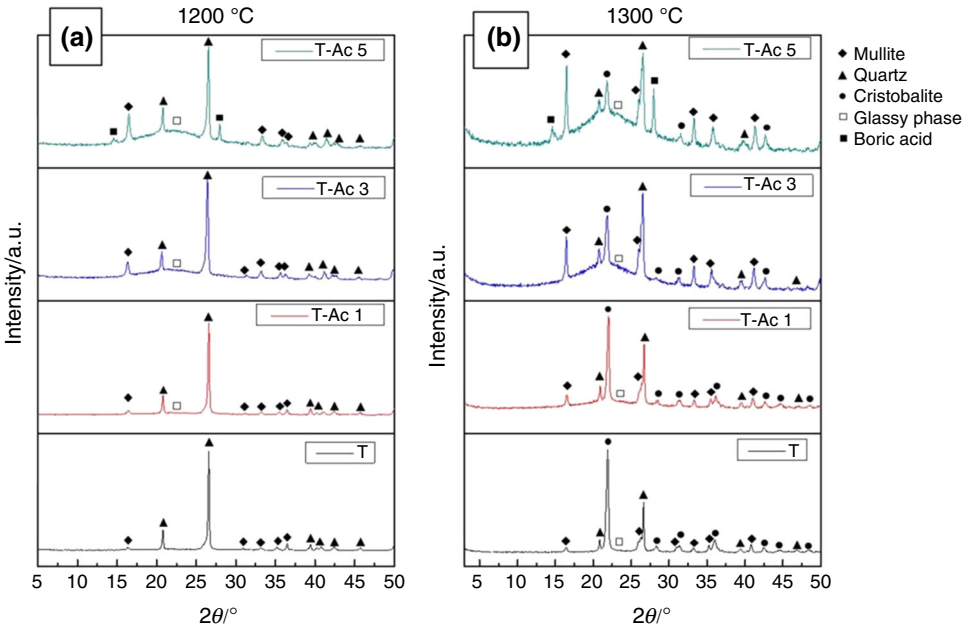

Fig. 8 XRD patterns of the Tincar clay (T) and clay–boric acid mixtures (T-Ac1; T-Ac3; T-Ac5) treated at 1200 and 1300 °C (**a** and **b**, respectively)

Table 3 Identified crystalline phases, chemical formula and employed PDF card

Crystalline phase	Formula	PDF card or method
Quartz	SiO_2	01-079-1910
Mullite	$3Al_2O_3{\cdot}2SiO_2$	01-079-1275
Cristobalite	SiO_2	01-082-0512
Boric acid	H_3BO_3	00-006-0297
Glassy phase	Silica (SiO_2) based	Le Bail method [29, 47]

actually a metalloid; in this case, the behavior is similar to metals. Boron is a glass former element [15]. It is worth to remember that the binary SiO_2–B_2O_3 phase system presents an eutectic temperature of approximately 500 °C.

The ternary system Al_2O_3–SiO_2–B_2O_3 was systematically studied by [53]. Several crystalline phases were identified and characterized. Boron mullite (formula) and related phases were identified and previously studied by Zhang et al. [54]. Hence, the mullite identified phase is actually a B-mullite phase [15].

The results of the Rietveld refinement and PDF cards for each phase are shown and compared in Table 3.

The lattice parameters of quartz show no difference within the studied samples. As mentioned, two lattice parameters were employed for the cristobalite refinement. Boric acid lattice parameters do not present important differences as well. A clear tendency was observed in the mullite lattice parameters. All three (*a*—mullite $3Al_2O_3$-$2SiO_2$, *b*—cristobalite SiO_2, *c*—quartz SiO_2) lattice parameters decrease with the addition of boric acid in the initial formulation. Luhrs et al. [15] and Zhang [54] systematically studied the boron mullite crystallographic features of B-mullite synthetized by a gel route. They found that the lattice parameter *c* strongly depends on the initial boron content of the precursor and proposed to use this parameter as a relative measure for the amount of boron in mullite up to 10%.

In Fig. 9, the lattice parameter *c* is plotted as a function of the boron % molar content of the studied samples. In the same plot, the *c* mullite lattice parameters of Luhrs and Zhang studies are plotted as well. In those studies, all the added B_2O_3 is incorporated to the mullite samples in a stoichiometric way.

In the present clay-based materials, a fraction of the introduced B_2O_3 is part of the silica-based glassy phase and the other fraction is incorporated to the mullite phase.

Additionally, the presence of quartz and cristobalite should be taken into account. After analyzing the lattice parameters of these phases, no boron solid solution can be presumed.

These facts explain the observed differences.

From the Rietveld refinement including glassy phase with the Le Bail approach, a phase quantification of the eight studied samples was performed.

Figure 10 presents the phase composition evaluated by the Rietved method. Global estimated standard deviations were below 2 mass%. In all cases, they were derived from the estimated standard deviation on individual scale factors, for the respective phases.

The goodness of the Rietveld refinement is usually represented by the Rwp parameter [ref]. The Rwp values are adequate (Rwp $\leq$ 15 in all the cases) and similar to the ones achieved in similar materials [1, 50, 51, 55, 56]. No boron-containing crystalline phases were detected.

Table 4 Cell parameters of the different phases in the materials

	a	Err	*b*	Err	*c*	Err
Quartz PDF card: 01-079-1910						
T-1200	4.91957	0.00039	4.91957	0.00039	5.40639	0.00011
T-1300	4.91059	0.00077	4.91059	0.00077	5.40160	0.00026
T-Ac1 1200	4.92002	0.00056	4.92002	0.00056	5.40779	0.00016
T-Ac1 1300	4.91185	0.00092	4.91185	0.00092	5.40378	0.00031
T-Ac3 1200	4.92950	0.00161	4.92950	0.00161	5.41662	0.00046
T-Ac3 1300	4.92438	0.00274	4.92438	0.00274	5.41634	0.00154
T-Ac5 1200	4.92169	0.00084	4.92169	0.00084	5.42165	0.00029
T-Ac5 1300	4.91927	0.00180	4.91927	0.00180	5.43009	0.00068
Mullite PDF card: 01-079-1275						
T-1200	7.55366	0.00204	7.69860	0.00022	2.88688	0.00005
T-1300	7.54595	0.00158	7.69305	0.00017	2.88315	0.00005
T-Ac1 1200	7.54583	0.00291	7.68126	0.00031	2.86722	0.00008
T-Ac1 1300	7.53894	0.00202	7.68724	0.00022	2.87025	0.00007
T-Ac3 1200	7.52306	0.00469	7.66307	0.00043	2.84038	0.00012
T-Ac3 1300	7.53486	0.00347	7.67943	0.00397	2.85371	0.00098
T-Ac5 1200	7.51011	0.00457	7.65758	0.00439	2.82515	0.00075
T-Ac5 1300	7.51853	0.00205	7.65641	0.00328	2.82657	0.00023
Cristobalite 1						
T-1200	–	–	–	–	–	–
T-1300	4.99813	0.00141	4.99813	0.00141	6.98815	0.00084
T-Ac1 1200						
T-Ac1 1300	5.01074	0.00288	5.01074	0.00288	7.00947	0.00202
T-Ac3 1200	–	–	–	–	–	–
T-Ac3 1300	5.01949	0.00000	5.01949	0.00000	6.94666	0.00533
T-Ac5 1200	–	–	–	–	–	–
T-Ac5 1300	5.02246	0.00625	5.02246	0.00625	6.95882	0.00479
Cristobalite 2 PDF card: 01-082-0512						
T-1200	–	–	–	–	–	–
T-1300	4.97139	0.00093	4.97139	0.00093	6.92366	0.00056
T-Ac1 1200	–	–	–	–	–	–
T-Ac1 1300	4.97220	0.00154	4.97220	0.00154	6.94113	0.00091
T-Ac3 1200	–	–	–	–	–	–
T-Ac3 1300	4.99700	0.00000	4.99700	0.00000	7.07000	0.00000
T-Ac5 1200	–	–	–	–	–	–
T-Ac5 1300						
Boric acid PDF card: 00-006-0297						
T-Ac5 1200	7.04466	0.00994	7.06406	0.01069	6.58303	0.00296
T-Ac5 1300	7.03787	0.00447	7.05139	0.00498	6.58733	0.00154

The values were obtained by Rietveld refinement of the DRX patterns

The presence of boric acid in high T-Ac5 sample evidences a partial rehydration of the boron oxide in the glassy phase. Hence, the amount of boric acid is restricted below this proportion.

The difference of mullite, quartz, cristobalite and glassy phase change with the explored variables (temperature and additive content) can easily be observed in the bar chart (Fig. 10).

The mullite (and boron mullite) content is around 24 and 27%, for samples fired at 1200 and 1300 °C, respectively. On the other side, the boric acid addition decreases the amount of mullite phase and simultaneously increases the amount of glassy phase. A 70% of glassy phase is achieved. The resultant amount of silica-based phases (quartz and cristobalite) decreases with the addition of boric acid.

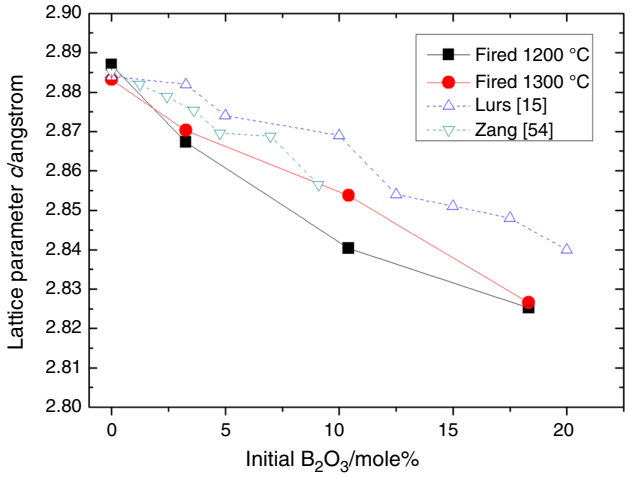

Fig. 9 Refined *c* lattice parameter of mullite phase (PDF 01-079-1275) for the studied samples fired at 1200 and 1300 °C as a function of boric acid proportion. Luhrs et al. [15] and Zhang et al. [54] values are plotted as well

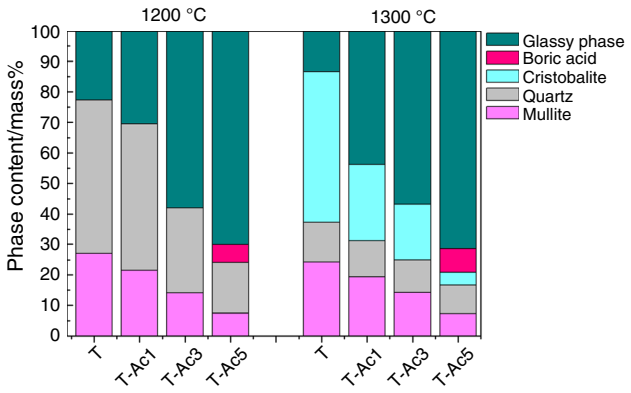

Fig. 10 Crystalline and non-crystalline phase content of the studied samples as a function of the initial composition and the firing temperature

Microstructure analysis of ceramics fired at 1300 °C by scanning electron microscope

The developed microstructures, after firing the clay and clay–boric acid mixtures at 1300 °C, were evaluated by means of scanning electron microscopy; the relatively dense and complex microstructure of the ceramics is revealed (Fig. 11). In images with lower magnification (× 100 images: a, d, g and J), pores (in black) can be identified in the matrix (different shades of gray). Chemical etching was carried out in the × 1000 and × 2000 micrographs (a, b, c, e, f, h, i, k and l), and this permits to observe the crystalline grains.

Compared to the pure clay-based material (T), the observed macroporosity decreases with the 1 mass% H_3BO_3 addition. Higher incorporations result in an increase in the observed pore amount, and this was also observed in the immersion test (Fig. 6).

The matrix can be described as a complex microstructure of crystalline grains (several microns) embedded in the glassy (amorphous–viscous) continuous phase. Grains correspond to the crystalline phases detected by XRD: mullite, quartz and cristobalite. The glassy phase, predominantly silica based, was also observed. Poris correlated with the boron addition and follows the T–T < T-Ac1 < T-Ac3 ≈ T-Ac 5 sequence, as evaluated by the Archimedes method (Fig. 6). Rounded macro-pores (≈ 100 μm) are complemented by a micro (meso)-porosity only observed in greater magnifications. The observed microstructures are equivalent to those extensively reported in the literature [3, 8, 48, 57].

The performed chemical etching permits to easily observe the grain morphology of the crystalline phases. The so-called primary mullite presents slightly elongated rounded morphology, and the secondary mullite presents needles [58, 59]. It is well known that the mullite phase governs the mechanical properties of the clay-based ceramic materials, usually known as the "mullite hypothesis." This fact is related to the mullite needle morphology and the compressive stress that its grains undergo during the cooling thermal processing cycles [1, 9, 59, 60]. The amount of secondary mullite differs considerably between the studied samples, the pure clay presents only primary mullite, and the boron-containing samples present important amount of secondary mullite.

This is evidence of a change in the mullite formation mechanism. This corresponds with the thermal analysis performed (Figs. 4, 5), where, for the binary mixtures, the boron presence resulted in the disappearance of the SAS-primary mullite exothermic peak (≈ 980 °C). This might present consequences in the mechanical behavior of clay-based materials if processed with boric acid as fluxing agent.

It is also worth to point out the observed decrease in the mullite amount, and this is probably restricted to the amount of available aluminum oxide, which decreased by two reasons: firstly, a dilution effect due the incorporation of boric acid in the initial formulation, and secondly, due to the alumina presence in the glassy phase.

After this, the boric acid role could be summarized as a glassy phase promoter and glass-forming material; from this glass, the secondary mullite crystallizes with needle morphologies with a potential reinforcement behavior.

This is concordant with the thermal tests carried out. The mentioned primary mullite formation suppression (Fig. 4) and the optimum sintering were observed in the dilatometric tests, which were not observed in the pure clay test up to 1400 °C and observed in the binary mixtures (Fig. 5). This is also in accordance with previous works

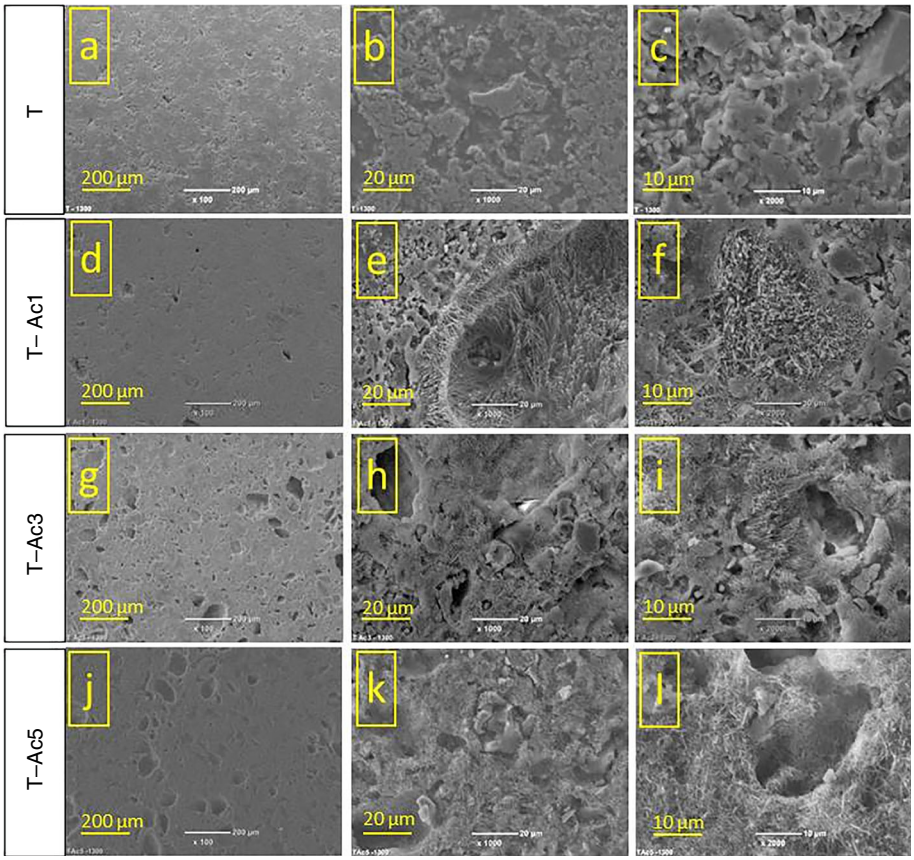

Fig. 11 SEM images of the clay (**a**, **b**, **c**) and clay–boric acid mixtures fired at 1300 °C (T-Ac1 **d**, **e**, **f**; T-Ac3 **g**, **h**, **i**; T-Ac5 **j**, **k**, **l**)

where boron-containing materials were incorporated [24, 61].

Conclusions

The boric acid does not interfere in the dehydration temperature of the kaolinitic clay for both the surface and structural water losses. On the contrary, the spinel and mullite formation temperatures (980 °C and 1100–1250 °C, respectively) were modified. The thermal signals become wider and occur at lower temperatures, when boric acid proportion increases, evidencing a mechanism change for both processes.

The amount of glass was strongly increased by the boron incorporation. X-ray diffraction, supplemented by Rietveld refinement, verified the presence and thermal evolution of crystalline and glassy phases. Identified mullite phases consisted in mullite and boron mullite solid solutions. The amount of mullite was slightly decreased by a dilution effect of the boric acid in the formulation. Some boric acid was observed evidencing a rehydration of higher added samples. The mullite cell parameters allowed to observe the amount of boron incorporation in the mullite phase. The *c* lattice parameter decreased with the initial boric acid content from 2.85 to 2.82 Å. This was not influenced by the firing temperature, inferring that the solid solution is formed at lower temperatures.

Dense materials were satisfactorily processed through a dry scalable process. The open porosity was slightly high. This can be optimized by the addition of other fluxing agents like feldspars or earthen alkali sources.

The present study gives information for further clay-based materials design with boron oxide as fluxing agent. The dry route hypothesis was confirmed. Both formulation and firing programs can be optimized. High boron addition (5 mass%) is not recommended due to the observed partial rehydration.

Acknowledgements MFH, MAV and MFS acknowledge CONICET for the fellowships. This work has been partially supported by Nano-Petro FONARSEC Project 2012 (ANPCyT). PICT-2016-1193 (2017–2020) (ANPCyT) and PIO CONICET-UNLA 2016–2018. Nro: 22420160100023CO (CONICET).

References

1. Serra MF, Conconi MS, Suarez G, Agietti EF, Rendtorff NM. Firing transformations of an argentinean calcareous commercial clay. Ceramica. 2013;59:254–61.

2. Dondi M, Raimondo M, Zanelli C. Clays and bodies for ceramic tiles: reappraisal and technological classification. Appl Clay Sci. 2014;96:91–109.
3. Chakraborty AK. Phase transformation of kaolinite clay. Springer, New Delhi; 2014. http://dx.doi.org/10.1007/978-81-322-1154-9.
4. Chandrasekhar S, Ramaswamy S. Influence of mineral impurities on the properties of kaolin and its thermally treated products. Appl Clay Sci. 2002;21:133–42.
5. Liu P. Polymer modified clay minerals: a review. Appl Clay Sci. 2007;38:64–76.
6. Liu X-J, Sun XW, Zhang JJ, Pu XP, Ge QM, Huang LP. Fabrication of β-sialon powder from kaolin. Mater Res Bull. 2003;38:1939–48.
7. She JH, Ohji T. Fabrication and characterization of highly porous mullite ceramics. Mater Chem Phys. 2003;80:610–4.
8. Iqbal Y, Lee WE. Microstructural evolution in triaxial porcelain. J Am Ceram Soc. 2000;83:3121–7.
9. Carty WM, Senapati U. Porcelain—raw materials, processing, phase evolution, and mechanical behavior. J Am Ceram Soc. 1998;81:3–20.
10. Liang F, Sayed M, Al-Muntasheri GA, Chang FF, Li L. A comprehensive review on proppant technologies. Petroleum. 2016;2:26–39.
11. Agrafiotis C, Tsoutsos T. Energy saving technologies in the European ceramic sector: a systematic review. Appl Therm Eng. 2001;21:1231–49.
12. Bovea MD, Díaz-Albo E, Gallardo A, Colomer FJ, Serrano J. Environmental performance of ceramic tiles: improvement proposals. Mater Des. 2010;31:35–41.
13. Sánchez E, García-Ten J, Sanz V, Moreno A. Porcelain tile: almost 30 years of steady scientific-technological evolution. Ceram Int. 2010;36:831–45.
14. Kartal A, Arpaozu A. Effects of a boron containing calcination product to porcelains on the final properties. Key Eng Mater. 2004; https://www.scientific.net/KEM.264-268.1653. Accessed 15 Aug 2018.
15. Lührs H, Fischer RX, Schneider H. Boron mullite: formation and basic characterization. Mater Res Bull. 2012;47:4031–42.
16. Kavas T. Use of boron waste as a fluxing agent in production of red mud brick. Build Environ. 2006;41:1779–83.
17. Harabi A, Guerfa F, Harabi E, Benhassine M-T, Foughali L, Zaiou S. Preparation and characterization of new dental porcelains, using K-feldspar and quartz raw materials. Effect of B_2O_3 additions on sintering and mechanical properties. Mater Sci Eng, C. 2016;65:33–42.
18. Olgun A, Erdogan Y, Ayhan Y, Zeybek B. Development of ceramic tiles from coal fly ash and tincal ore waste. Ceram Int. 2005;31:153–8.
19. Kurama S, Kara A, Kurama H. The effect of boron waste in phase and microstructural development of a terracotta body during firing. J Eur Ceram Soc. 2006;26:755–60.
20. Richerson DW. Modern ceramic engineering: properties, processing, and use in design. 3rd ed. Boca Raton: CRC Press; 2005.
21. A Preparação a Seco de Massas Cerâmicas. http://scholar.googleusercontent.com/scholar?q=cache:Pb1zWeSvOa8J:scholar.google.com/&hl=es&as_sdt=0,5. Accessed 15 Aug 2018.
22. Sousa SJG, Holanda JNF. Development of red wall tiles by the dry process using Brazilian raw materials. Ceram Int. 2005;31:215–22.
23. Dondi M. Feldspathic fluxes for ceramics: sources, production trends and technological value. Resour Conserv Recycl. 2018;133:191–205.
24. Akpinar S, Evcin A, Ozdemir Y. Effect of calcined colemanite additions on properties of hard porcelain body. Ceram Int. 2017;43:8364–71.
25. Bragança SR, Bergmann CP. Waste glass in porcelain. Mater Res. 2005;8:39–44.
26. Dominguez E, Cravero F. Los recursos de caolín de Chubut y Santa Cruz. Recur Miner Repúb Argent. Zappettini E.O. Argentina: Instituto de Geología y Recursos Minerales. Secretaría de Estado de Geología y Minería de Argentina; 1999. p. 1265–1272.
27. Bish DL, Post JE. Quantitative mineralogical analysis using the Rietveld full-pattern fitting method. Am Mineral. 1993;78:932–40.
28. Bish DL, Howard SA. Quantitative phase analysis using the Rietveld method. J Appl Crystallogr. 1988;21:86–91.
29. Le Bail A. Modelling the silica glass structure by the Rietveld method. J Non Cryst Solids. 1995;183:39–42.
30. Quantitative analysis of silicate glass in ceramic materials by the rietveld method. http://www.ing.unitn.it/∼luttero/Publications/EPDIC_V/silicate_glass.html. Accessed 16 Feb 2018.
31. MacKenzie KJD, Meinhold RH, Brown IWM, White GV. The formation of mullite from kaolinite under various reaction atmospheres. J Eur Ceram Soc. 1996;16:115–9.
32. Okada K, ŌTsuka N, Ossaka J. Characterization of spinel phase formed in the kaolin–mullite thermal sequence. J Am Ceram Soc. 1986;69:C-251–3.
33. Sanz J, Madani A, Serratosa JM, Moya JS, Aza S. Aluminum-27 and silicon-29 magic-angle spinning nuclear magnetic resonance study of the kaolinite-mullite transformation. J Am Ceram Soc. 1988;71:C418–21.
34. Schneider H, Schreuer J, Hildmann B. Structure and properties of mullite—a review. J Eur Ceram Soc. 2008;28:329–44.
35. De Aza AH, Turrillas X, Rodriguez MA, Duran T, Pena P. Time-resolved powder neutron diffraction study of the phase transformation sequence of kaolinite to mullite. J Eur Ceram Soc. 2014;34:1409–21.
36. Sevim F, Demir F, Bilen M, Okur H. Kinetic analysis of thermal decomposition of boric acid from thermogravimetric data. Korean J Chem Eng. 2006;23:736–40.
37. Hernández MF, Suárez G, Cipollone M, Conconi MS, Aglietti EF, Rendtorff NM. Formation, microstructure and properties of aluminum borate ceramics obtained from alumina and boric acid. Ceram Int. 2017;43:2188–95.
38. Gielisse PJM, Foster WR. The system Al_2O_3–B_2O_3. Nature. 1962;195:69–70.
39. Hernández MF, Suárez G, Cipollone M, Aglietti EF, Rendtorff NM. Mechanical behavior and microstructure of porous needle: aluminum borate ($Al_{18}B_4O_{33}$) and Al_2O_3–$Al_{18}B_4O_{33}$ composites. Ceram Int. 2017;43:11759–65.
40. Zanelli C, Raimondo M, Guarini G, Dondi M. The vitreous phase of porcelain stoneware: composition, evolution during sintering and physical properties. J Non Cryst Solids. 2011;357:3251–60.
41. Dondi M, Iglesias C, Dominguez E, Guarini G, Raimondo M. The effect of kaolin properties on their behaviour in ceramic processing as illustrated by a range of kaolins from the Santa Cruz and Chubut Provinces, Patagonia (Argentina). Appl Clay Sci. 2008;40:143–58.
42. Decterov SA, Swamy V, Jung I-H. Thermodynamic modeling of the B_2O_3–SiO_2 and B_2O_3–Al_2O_3 systems. Int J Mater Res. 2007;98:987–94.
43. Hammel EC, Ighodaro OL-R, Okoli OI. Processing and properties of advanced porous ceramics: an application based review. Ceram Int. 2014;40:15351–70.
44. Smith DS, Alzina A, Bourret J, Nait-Ali B, Pennec F, Tessier-Doyen N, et al. Thermal conductivity of porous materials. J Mater Res. 2013;28:2260–72.
45. Studart AR, Gonzenbach UT, Tervoort E, Gauckler LJ. Processing routes to macroporous ceramics: a review. J Am Ceram Soc. 2006;89:1771–89.

46. Meille S, Lombardi M, Chevalier J, Montanaro L. Mechanical properties of porous ceramics in compression: on the transition between elastic, brittle, and cellular behavior. J Eur Ceram Soc. 2012;32:3959–67.
47. Butler MA, Dyson DJ. The quantification of different forms of cristobalite in devitrified alumino-silicate ceramic fibres. J Appl Crystallogr. 1997;30:467–75.
48. Hernández MF, Conconi MS, Cipollone M, Herrera MS, Rendtorff NM. Ceramic behavior of ball clay with gadolinium oxide (Gd2O3) addition. Appl Clay Sci. 2017;146:380–7.
49. Madsen IC, Finney RJ, Flann RCA, Frost MT, Wilson BW. Quantitative analysis of high-alumina refractories using X-ray powder diffraction data and the rietveld method. J Am Ceram Soc. 1991;74:619–24.
50. Andrini L, Gauna MR, Conconi MS, Suarez G, Requejo FG, Aglietti EF, et al. Extended and local structural description of a kaolinitic clay, its fired ceramics and intermediates: an XRD and XANES analysis. Appl Clay Sci. 2016;124–125:39–45.
51. Conconi MS, Gauna MR, Serra MF, Suarez G, Aglietti EF, Rendtorff NM. Quantitative firing transformations of a triaxial ceramic by X-ray diffraction methods. Ceramica. 2014;60:524–31.
52. Kolitsch U, Seifert HJ, Aldinger F. Phase relationships in the system Gd_2O_3–Al_2O_3–SiO_2. J Alloys Compd. 1997;257:104–14.
53. Swamy V, Jung I-H, Decterov SA. Thermodynamic modeling of the Al_2O_3–B_2O_3–SiO_2 system. J Non Cryst Solids. 2009;355:1679–86.
54. Zhang G, Fu Z, Wang Y, Wang H, Wang W, Zhang J, et al. Boron-doped mullite derived from single-phase gels. J Eur Ceram Soc. 2010;30:2435–41.
55. Bonetto RD, Zalba PE, Conconi MS, Manassero M. The Rietveld method applied to quantitative phase analysis of minerals containing disordered structures. Rev Geol Chile. 2003;30:103–15.
56. Hillier S. Accurate quantitative analysis of clay and other minerals in sandstones by XRD: comparison of a Rietveld and a reference intensity ratio (RIR) method and the importance of sample preparation. Clay Miner. 2000;35:291–302.
57. Lee HK, Zerbetto S, Colombo P, Pantano CG. Glass-ceramics and composites containing aluminum borate whiskers. Ceram Int. 2010;36:1589–96.
58. Lee WE, Souza GP, McConville CJ, Tarvornpanich T, Iqbal Y. Mullite formation in clays and clay-derived vitreous ceramics. J Eur Ceram Soc. 2008;28:465–71.
59. Hernández MF, Suárez G, Baudin C, Pena Castro P, Aglietti EF, Rendtorff NM. Densification of lightweight aluminum borate ceramics by direct sintering of milled powders. J Asian Ceram Soc. 2018;6(4):374–83.
60. Romero M, Pérez JM. Relation between the microstructure and technological properties of porcelain stoneware. A review. Mater Constr. 2015;65:e065.
61. Bayca SU. Effects of the addition of ulexite to the sintering behavior of a ceramic body. J Ceram Process Res. 2009;10:162–6.